

Investigation of Attenuation of the Lg -Wave Amplitude in the Caribbean Region

by M. Hosseini,* S. Pezeshk, A. Haji-Soltani, and M. Chapman

Abstract The focus of this study is to determine the frequency-dependent quality factor function $Q(f)$ for the Caribbean region. The analysis considers the Lg portion of 2685 three-component waveforms. Waveforms are selected from 116 earthquakes that occurred between 2006 and 2013 with moment magnitude M_w ranging from 4.6 to 7.0. Spectral amplitudes over 12 distinct passbands from 0.1 to 12.8 Hz are calculated only for waveforms with a signal-to-noise ratio of 5 or better. In the regression model, the vertical component and the geometric mean of two horizontal components are used to estimate $Q(f)$. A geometrical spreading function with spectral amplitude decay of $R^{-0.5}$ is used for distances beyond 100 km. The following quality factor functions for the assumed geometrical spreading are obtained: $Q^H = 310f^{0.54}$ for the horizontal components, and $Q^V = 235f^{0.65}$ for the vertical components.

Introduction

Currently, there are limited ground-motion prediction equations (GMPEs) for the southeastern United States and the northern Caribbean region. One possible approach for developing GMPEs for this region is to estimate ground motions by using a stochastic procedure (Atkinson and Boore, 1995, 1998, 2006; Frankel *et al.*, 1996; Toro *et al.*, 1997; Boore, 2003; Pezeshk *et al.*, 2011). Critical to any stochastic simulation is the selection of seismological input parameters such as the frequency-dependent quality factor function $Q(f)$. The purpose of this study is to determine the frequency-dependent quality factor function $Q(f)$ for the Caribbean region. The shaking intensity of earthquakes and instrumental seismic recordings in the different tectonic environments show that areas of active tectonics, like the Caribbean and the western United States (WUS) regions, have higher attenuation (lower quality factor) of seismic waves than the stable continental regions such as the central and eastern United States (CEUS) regions (Aki, 1980a,b; Singh and Herrmann, 1983; Frankel *et al.*, 1990; Benz *et al.*, 1997; Erickson *et al.*, 2004; Zandieh and Pezeshk, 2010; Zhou *et al.*, 2011; McNamara *et al.*, 2012). McNamara *et al.* (2012), based on studies by Aki (1980a,b), Gregersen (1984), Frankel (1991), and Benz *et al.* (1997), suggested these observations from different tectonic regions indicate a highly fractured crust in tectonically active regions that absorb high-frequency seismic waves, differences in crustal temperature, and variations in crustal structure.

Lg waves carry the most prominent energy for continental paths at regional distances (Báth, 1954). Lg was first identified as surface waves (Press and Ewing, 1952), which are S waves

trapped in the crustal waveguide. The amplitude of Lg waves in the continental crust is a function of crustal structure and the physical properties of the crustal material (Mitchell, 1995). Lg waves are attenuated more rapidly in active tectonic regions, in contrast with the stable tectonic blocks (Aki, 1980a,b; Zhou *et al.*, 2011). The dominant frequency of Lg is in the range of 0.5–5.0 Hz, with group velocity of approximately 2.8–3.7 km/s.

The Caribbean study region is made up of over 7000 islands, islets, coral reefs, and cays. The independent countries of the region are Cuba, Dominican Republic, Haiti, the Bahamas, Jamaica, and Trinidad and Tobago. The Caribbean lithospheric plate mainly consists of an anomalously thick, oceanic plateau located between two major continental regions. It is a geologically complex region that exhibits a variety of plate boundary interactions, including subduction (Lesser Antilles and central America) and strike slip on northern and southern boundaries, and seafloor spreading in the Cayman Trough (Mattson, 1977; Jackson, 2002). The Port-au-Prince region of Haiti was struck by an earthquake of M_w 7.0 on 12 January 2010. Damages caused by this disastrous earthquake, in which more than 200,000 people were killed, were estimated to be around \$8 billion (Calais *et al.*, 2010).

Many studies have been performed to evaluate the attenuation characteristics of seismic waves in various regions of the world (e.g., Nuttli, 1973; Mitchell, 1975; Bollinger, 1979; Chen and Pomeroy, 1980; Nicolas *et al.*, 1982; Atkinson and Mereu, 1992; Atkinson and Boore, 1995; Benz *et al.*, 1997; Atkinson, 2004; Allen *et al.*, 2007; Zandieh and Pezeshk, 2010). A number of attenuation studies have also been carried out for the Caribbean region. Molnar and Oliver (1969) investigated the average attenuation of high-frequency S_H shear waves propagating across the concave side of the

*Now at URS Corporation, Los Angeles, California 90017.

Antilles arc for both oceanic and continental crust. They reported anomalous propagation of shear waves near the Lesser Antilles. Rial (1976) estimated the shear-wave Q for propagation paths through the anomalous zone to be about 400 for the entire path. According to Rial (1976), seismograms for paths through the anomalous region feature frequencies of 0.5 or less, and Q is about 80 or less, agreeing with Molnar and Oliver (1969). Frankel (1982) reported Q of about 400 for Rayleigh waves for Caribbean region. Ambe and Lynch (1993) investigated coda quality factor Q_c for the eastern Caribbean. He reported Q_c in the range from 152 to 239 at 1.5 Hz in the eastern Caribbean, increasing to approximately 1236–3455 at 16 Hz. Ambe and Lynch (1993) estimated Q_0 in the range of 97–145, with η in the 0.82–1.09 range in the linear logarithmic regression $Q = Q_0 f^\eta$. Recently, McNamara *et al.* (2012) estimated Q using approximately 850 observations of Lg waves in the Hispaniola Island region. They used a hinged-trilinear geometrical spreading function consistent with Atkinson (2004) and Motazedian and Atkinson (2005). Their result was $Q(f) = 245(\pm 31)f^{0.61(\pm 0.082)}$ and $Q(f) = 224(\pm 27)f^{0.64(\pm 0.073)}$ for vertical and horizontal components, respectively.

At distances less than 100 km, the attenuation is dominated by geometrical spreading (Nuttli, 1973; Atkinson, 2012; McNamara *et al.*, 2012). At distances greater than 100 km, frequency-dependent attenuation associated with $Q(f)$ becomes important. Determination of Q is a difficult problem. In some cases, data are insufficient to experimentally isolate geometrical spreading and Q , resulting in a trade-off between the estimate of anelastic attenuation (frequency-dependent Q) and the geometrical spreading. Estimates of Q may depend on assumptions concerning geometrical spreading (Atkinson and Mereu, 1992; Atkinson, 2012). Atkinson (2004) reported a geometrical spreading of $R^{-1.3}$ for distances less than 70 km, $R^{+0.2}$ for between 70 and 140 km, and $R^{-0.5}$ for distances beyond 140 km. Zandieh and Pezeshk (2010) reported $R^{-1.0}$ for distances less than 70 km, $R^{+0.25}$ for between 70 and 140 km, and $R^{-0.5}$ for distances beyond 140 km for the Mississippi Embayment. Motazedian and Atkinson (2005) adopted a hinged-trilinear functional form specific to Puerto Rico, where geometrical spreading is described by $R^{-1.0}$, R^0 , and $R^{-0.5}$, with hinge points at 75 and 100 km.

Chapman and Godbee (2012) modeled synthetic seismograms for strike-slip and reverse focal mechanisms for stations at different distances and azimuths. Different source depths were used in the analysis, and they generated both horizontal and vertical ground accelerations within 120 km of the source, considering horizontally layered velocity models for eastern North America. They observed the behavior of the geometric mean of the randomly oriented horizontal components differed from the vertical-component ground accelerations. They reported the amplitude decay of vertical components (averaged over all azimuths) at stations in the range $1.5h < R < 60$ km, in which h is the focal depth, ranges from $R^{-1.5}$ to $R^{-4.0}$, and this rate is more rapid for deeper focal depths and systematically more rapid for reverse focal

mechanisms. From 60 to 120 km, no decay was observed for vertical S -wave amplitudes due to reflections from the mid-crust. The decay rate for horizontal amplitude components (averaged over all azimuths) for distances less than 60 km, is $R^{-1.3}$ for strike slip and $R^{-1.5}$ for reverse-faulting mechanisms, without apparent dependence on the source depth (Chapman and Godbee, 2012).

This study consists of a database of 2685 seismograms from 116 earthquakes with moment magnitude M_w from 4.6 to 7.0 that occurred from 2006 to 2013. The most notable event in the database is the M_w 7.0 earthquake that struck the Port-au-Prince region of Haiti on 12 January 2010. Figure 1 shows the distribution of earthquakes and seismic stations used in this study; only events and recording stations in the Caribbean plate are used. The effect of crustal structure, and particularly transitions in crustal structure, has a first-order effect on Lg -wave attenuation. As pointed out by many of the references (e.g., Kennett, 1986; Erickson *et al.*, 2004), the attenuation properties of Lg waves are very different in different crustal structures, and it is strongly affected by transitions in crustal structure. Erickson *et al.* (2004) points out that Lg waves can completely attenuate within 500 km in California, whereas they can be seen at distances up to 6000 km in North Africa. Kennett (1986) shows that Lg waves are particularly strongly affected by ocean–continent transitions and that oceanic paths strongly affect them.

Seismic activity in the northeastern Caribbean region is cooperatively monitored by the Puerto Rico Seismic Network (PRSN) and the Puerto Rico Strong Motion Program (PRSMMP). The PRSMMP operates both structural array and free-field stations whereas the PRSN maintains vault stations (Clinton *et al.*, 2006). Odum *et al.* (2013) selected 27 sites as the representative of the near-surface material to study the site parameters in Puerto Rico. They compared their results with the observed data for the 16 May 2010 M_w 5.8 Puerto Rico earthquake recorded in eight specific PRSMMP stations. The stations are located at distances from 0.5 to approximately 12 km from the surveyed sites (Odum *et al.*, 2013). A general geologic description of PRSMMP stations and their National Earthquake Hazards Reduction Program site classifications can be found in Odum *et al.* (2013). Also, Odum *et al.* (2013) provide V_{S30} obtained by reflection/refraction (body wave) and refraction microtremor (surface wave) surveys at sites near PRSMMP stations.

Data Selection and Preprocessing

For each earthquake, associated seismograms at a specific station are selected based on the availability of high-quality data. Only those seismograms recorded at hypocentral distances larger than 100 km and less than 1000 km are used for the regression analyses. Figure 2 illustrates the distribution of earthquakes in magnitude and distance.

Waveforms are recorded by broadband stations from the Caribbean (CU), Cayman Islands (CY), Instituto Sismológico Universitario (DR), Global Seismograph (IU), and Puerto

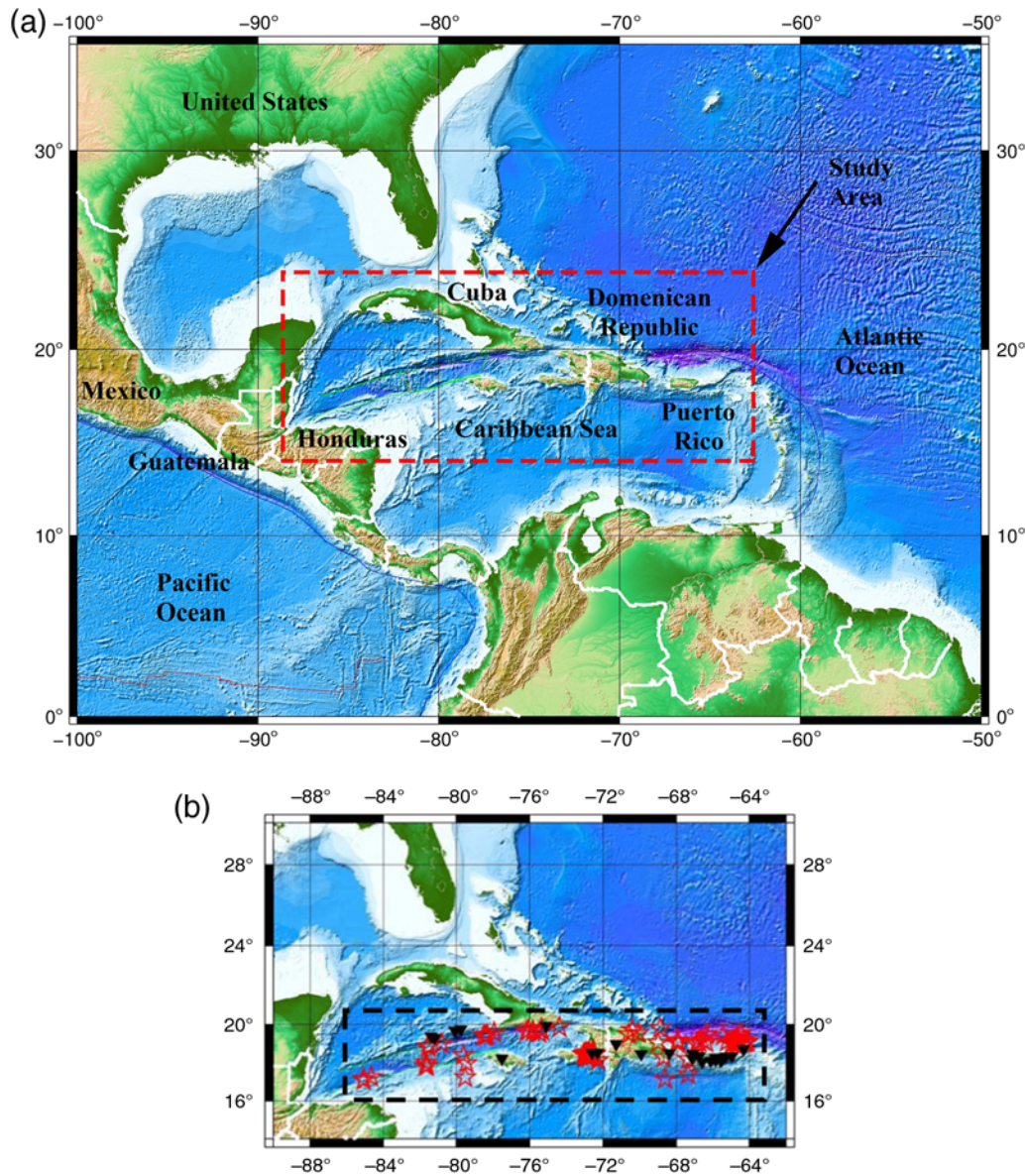


Figure 1. Maps of (a) the Caribbean region and (b) the study area, showing locations of earthquakes (stars) and broadband stations (inverted triangles). Only those earthquakes and stations in the Caribbean plate (inside the rectangle bordered by the dashed line in [b]) are used in this study. The color version of this figure is available only in the electronic edition.

Rico (PR) seismic networks. Waveforms are downloaded 30 s prior to and 600 s after the origin time of each earthquake, for all three components. A 30 s window before the event is used for signal-to-noise ratio control. The data preference is for broadband seismograms with high sample rates. Sampling rates are in the range of 20–100 points per second. The majority of dataset records have a sampling rate of 40 points per second and above. Based on the sampling rate of each specific waveform, the Nyquist frequency (f_{nyq} ; beyond which Fourier amplitudes are not used) ranges from 10 to 50 Hz. Table 1 presents the Nyquist frequency for different stations. The majority of stations have a constant sampling ratio according to time series from events. In contrast, about a third of the stations have different Nyquist frequency values due to different

sampling rate of time series from different events. Maximum and minimum of f_{nyq} is provided for these stations.

A fast Fourier transform (FFT) is used to derive the amplitude at 12 frequency bands, centering on 0.25, 0.35, 0.5, 0.7, 1.0, 1.4, 2.0, 2.8, 4.0, 5.6, 8.0, and 11.2 Hz. The lower limit of the first frequency band starts at 0.2 Hz and the upper limit of the last frequency band ends at 12.8 Hz. The bandwidth doubles every two intervals. For example, the first frequency band covers 0.2–0.3 Hz, the second band covers 0.3–0.4, the third covers 0.4–0.6, and so on.

After applying the FFT to the time series, amplitudes are averaged for frequencies falling in each frequency band, and their average amplitude is reported as the amplitude associated with the center frequency of that specific frequency

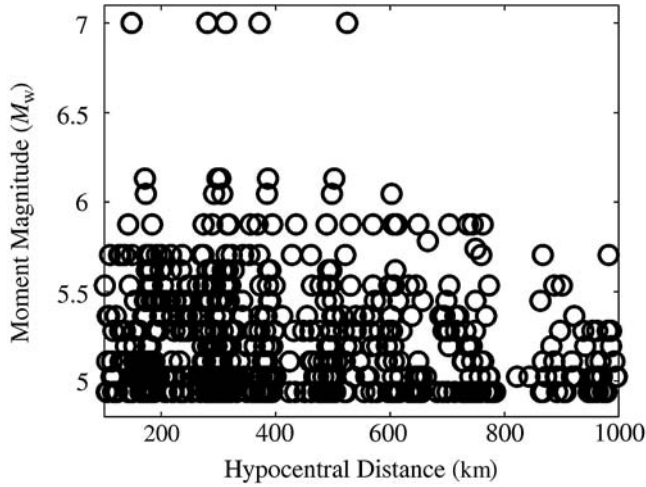


Figure 2. Moment magnitude versus distance plot for 116 events recorded at 25 stations.

band. Signal-to-noise considerations are implemented by considering noise in a 20 s window starting from 30 s prior to event time. The geometric mean of the two horizontal components is used along with the vertical component. FFT amplitudes for the noise window at the same 12 frequency centers are calculated and are compensated for the difference between data and noise window lengths. The data selection required signal-to-noise ratios of five or greater. FFT amplitudes are calculated for a data window capturing the L_g wave. Considering an L_g wavespeed of 3.50 km/s (McNamara *et al.*, 2012), L_g -wave arrival is defined as

$$T_{L_g} = T_0 + \frac{r}{3.50}, \quad (1)$$

in which T_{L_g} is the arrival time of the initial onset of the L_g phase, T_0 is the earthquake origin time, and r is the epicentral distance in kilometers. The duration window for the Fourier analysis of the L_g phase is defined by examination of the integral of the squared acceleration time series. The duration of the L_g window T_d is defined according to

$$\int_{T_{L_g}}^{T_{L_g}+T_d} a^2 dt = 0.75 \int_{T_{L_g}}^{T_{L_g}+150} a^2 dt, \quad (2)$$

in which a is the ground acceleration. The L_g signal duration (T_d) is defined as the time at which the integral of the squared acceleration time series (starting at T_{L_g}) reaches 75% of its value at $T_{L_g} + 150$ s. In the FFT analysis, we use the L_g window from T_{L_g} to $T_{L_g} + T_d$ to obtain the amplitudes in 12 frequency bands.

Figure 3 shows the location of stations AGPR and MPR, which recorded an event marked by the star. Seismograms from the 4 February 2008 earthquake with a reported magnitude of 5.5 recorded by these two stations are illustrated in Figure 4. At each station, all three components (BHE, BHN, and BHZ in order from top to bottom) are plotted, along with an L_g -wave window represented with vertical lines.

We performed data analysis separately for the geometric mean of amplitudes for the two horizontal components, as well as amplitudes for the vertical component, and each are reported separately. The next section provides details on the data analysis for the path effect study.

Data Analysis

Following Atkinson and Mereu (1992) and Zandieh and Pezeshk (2010), the spectral amplitude generated at the earthquake hypocenter (source amplitude) travels across the path between the source and the location of the recording seismograph. The source amplitude undergoes two major changes, one resulting from the path effect and the other from the local site geology at the location of the seismograph. The path effect is modeled by a combination of geometrical spreading and anelastic attenuation functions. Local site geology may amplify or deamplify the amplitude. The observed spectral amplitude is given by:

$$\log[O_{i,j}(f)] = \log[A_i(f)] - B(R_{i,j}) \log(R_{i,j}) - \frac{\log(e)\pi f}{Q(f) \times \beta} R_{i,j} + \log[S_j(f)], \quad (3)$$

Table 1
Nyquist Frequency of Different Stations

| Station Name | f_{nyq} (Hz) | Station Name | f_{nyq} (Hz) | Station Name | $\min(f_{nyq})$ (Hz) | $\max(f_{nyq})$ (Hz) |
|--------------|----------------|--------------|----------------|--------------|----------------------|----------------------|
| PR.PCDR | 10 | PR.ICMP | 20 | PR.AGPR | 10 | 20 |
| CU.GRTK | 20 | PR.IGPR | 20 | PR.AOPR | 10 | 20 |
| CU.GTBY | 20 | PR.MLPR | 20 | PR.CBYP | 10 | 20 |
| CU.MTDJ | 20 | PR.PDPR | 20 | PR.CDVI | 10 | 20 |
| CU.SDDR | 20 | PR.SMN1 | 20 | PR.CRPR | 10 | 20 |
| DR.SC01 | 20 | CN.JAKH | 50 | PR.ICM | 10 | 20 |
| PR.ABVI | 20 | CN.LGNH | 50 | PR.MPR | 10 | 20 |
| PR.CPD | 20 | CN.PAPH | 50 | PR.MTP | 10 | 20 |
| PR.CULB | 20 | CY.CBCY | 50 | PR.OBIP | 10 | 20 |
| PR.CUPR | 20 | CY.FSCY | 50 | PR.STVI | 10 | 20 |
| PR.EMPR | 20 | CY.LCCY | 50 | DR.SDD | 20 | 25 |
| PR.HUMP | 20 | CY.WBCY | 50 | | | |

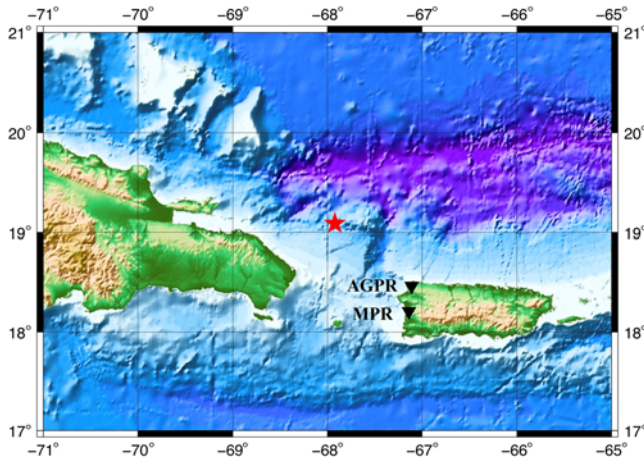


Figure 3. Locations of stations AGPR and MPR and the 4 February 2008 M_w 5.5 earthquake. The color version of this figure is available only in the electronic edition.

in which $O_{i,j}(f)$ is the observed spectral amplitude of earthquake i at station j at frequency f ; $A_i(f)$ is the source spectral amplitude of earthquake i at unit hypocentral distance; $B(R_{i,j})$ is the geometrical spreading coefficient; $R_{i,j}$ is the hypocentral distance; e is the Napier's constant (2.7183); $Q(f)$ is the quality factor, which is a function of the frequency; and S_j is the site (receiver) term for station j . It should be noted that the source spectral amplitude at the hypocenter location is considered to be equal for all of the observations at different stations and that the site (receiver) term S_j is independent of the event.

Geometrical Spreading

For a whole space, the concept of the geometrical spreading comes from the law of energy conservation where energy density on the surface of common-centered spheres with various diameters should decrease as the diameter increases. The geometrical spreading term, $B(R_{i,j}) \log R_{i,j}$ defines the logarithmic decay of amplitude at a specific frequency. Atkinson and Mereu (1992) modeled the geometrical spreading function using a hinged-trilinear functional form, in which the decay rate is different in three distance segments. The hinged-trilinear functional form of the geometrical spreading used here is given by

$$B(R_{i,j}) \log(R_{i,j}) = \begin{cases} b_1 \log R_{i,j} & R_{i,j} \leq R_1 \\ b_1 \log R_1 + b_2 \log R_{i,j}/R_1 & R_1 \leq R_{i,j} \leq R_2 \\ b_1 \log R_1 + b_2 \log R_2/R_1 + b_3 \log R_{i,j}/R_2 & R_{i,j} \geq R_2 \end{cases} \quad (4)$$

Motazedian and Atkinson (2005) and McNamara *et al.* (2012) used $b_1 = 1.0$, $b_2 = 0.0$, and $b_3 = 0.5$ with hinge points $R_1 = 75$ km and $R_2 = 100$ km. Our data is at distan-

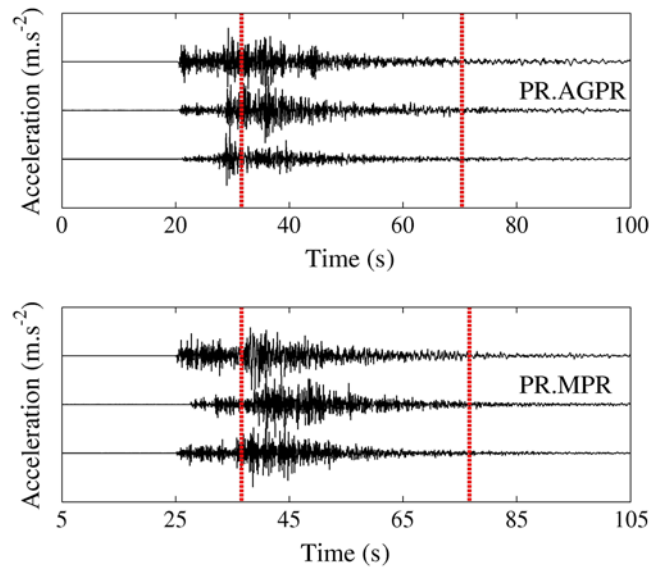


Figure 4. The 4 February 2008 earthquake (19.09° N, 67.92° W; 10 km depth; and M_w 5.5) recorded at (a) station AGPR, with a distance of 110.55 km, and (b) station MPR, with a distance of 128.3 km. For each station, three components of ground motion are shown: east–west, north–south, and vertical components. The color version of this figure is available only in the electronic edition.

ces greater than 100 km, and we assume the same model for geometrical spreading.

System of Equations

Rearranging equation (3) by considering a known geometrical spreading gives

$$\log[O_{i,j}(f)] + B(R_{i,j}) \log(R_{i,j}) = \log[A_i(f)] - \frac{\log(e)\pi f}{Q(f) \times \beta} R_{i,j} + \log[S_j(f)], \quad (5)$$

in which the left side consists of known parameters and the right side consists of unknown arguments. Equation (5) can be cast into a standard matrix formation,

$$\mathbf{Gm} = \mathbf{d}. \quad (6)$$

Equation (6) represents a typical linear inversion problem that can be solved using least squares, maximum-likelihood, or generalized inversion methods (e.g., Aki and Richards, 1980; Menke, 1984; Lay and Wallace, 1995; Aster *et al.*, 2013). The matrix \mathbf{G} is an $m \times n$ forward operator matrix; n is the number of unknowns (source terms, receiver terms, and the quality factor) and m is the number of observations. Such a system of equations has a unique solution when the number of observations (m) is more than or equal to the number of unknowns (n). The solution for \mathbf{m} is found using the singular value decomposition (SVD) procedure. The matrix \mathbf{G} can be expressed as the multiplication of three matrices:

$$\mathbf{G} = \mathbf{USV}', \quad (7)$$

in which \mathbf{S} is a diagonal matrix containing singular values of the matrix \mathbf{G} on its diagonal and has the same size as \mathbf{G} . Matrices \mathbf{U} and \mathbf{V} are $m \times m$ and $n \times n$ unitary square matrices, and the columns of each of them form a set of orthonormal vectors. The prime superscript for \mathbf{V} denotes the conjugate transpose. After finding the rank of the \mathbf{G} matrix, its pseudoinverse can be calculated as

$$\mathbf{G}^{-g} = \mathbf{V}_k \mathbf{S}_k^{-1} \mathbf{U}', \quad (8)$$

in which the subscript k denotes the consideration of the rank of \mathbf{G} in associated matrices, which includes removing problematic singular values from \mathbf{S} and their associated columns from \mathbf{U} and \mathbf{V} . Therefore, using the SVD procedure the vector \mathbf{m} can be written as (Menke, 1984)

$$\mathbf{m} = \mathbf{G}^{-g} \mathbf{d}. \quad (9)$$

Based on equation (5), if the total number of earthquakes is p and the total number of stations is q , then the matrices in equation (6) can be written as

$$\mathbf{G} = \begin{bmatrix} 1 & 0 & \dots & 0 & 1 & 0 & \dots & 0 & 0 & -\log(e)\pi f R_{11}/\beta \\ 1 & 0 & \dots & 0 & 0 & 1 & \dots & 0 & 0 & -\log(e)\pi f R_{12}/\beta \\ \vdots & \vdots \\ 0 & 0 & \dots & 1 & 0 & 0 & \dots & 1 & 0 & -\log(e)\pi f R_{p(q-1)}/\beta \\ 0 & 0 & \dots & 1 & 0 & 0 & \dots & 0 & 1 & -\log(e)\pi f R_{pq}/\beta \end{bmatrix}_{pq \times (p+q+1)},$$

$$\mathbf{m} = \begin{bmatrix} \log A_1(f) \\ \log A_2(f) \\ \vdots \\ \log A_{p-1}(f) \\ \log A_p(f) \\ \log S_1 \\ \log S_2 \\ \vdots \\ \log S_{q-1} \\ \log S_q \\ \frac{1}{Q(f)} \end{bmatrix}_{(p+q+1) \times 1}, \text{ and}$$

$$\mathbf{d} = \begin{bmatrix} \log[O_{11}(f)] + B(R_{11})\log(R_{11}) \\ \log[O_{12}(f)] + B(R_{12})\log(R_{12}) \\ \vdots \\ \log[O_{p(q-1)}(f)] + B(R_{p(q-1)})\log(R_{p(q-1)}) \\ \log[O_{pq}(f)] + B(R_{pq})\log(R_{pq}) \end{bmatrix}_{pq \times 1}. \quad (10)$$

Equations (9) and (10) are the basic equations for our inversion when the geometrical spreading term is known. Each row of the forward operator \mathbf{G} refers to an individual observation. The first p columns are related to earthquakes; columns $p + 1$ to $p + q$ address the receiver terms; and the very last column with index $p + q + 1$ is related to the frequency-dependent attenuation term. In an inversion problem, eigenvalues of \mathbf{G} affects the stability of the inversion and the accuracy of the results, that is, the ratio of largest eigenvalue to the smallest one, which is called the condition number, is an indicator of stability of the inversion. The smaller the condition number, the better the accuracy will be. In the case of the current study, when source terms are considered known, the SVD technique might not improve the accuracy all the time. However, in case of unknown source terms, improvement was observed in most of the cases where the interplay between the source and site (receiver) terms are resolved effectively.

For example, in the inversion for the quality factor at the 8.0 Hz frequency for the vertical component, \mathbf{G} is a 145×16 matrix (145 observed data and 16 unknown model parameters); and, after SVD, the eigenvalues are plotted in Figure 5.

For the current example, the results of the SVD technique become the same as those from the least square solution (Fig. 6).

Source Model

The source acceleration Fourier amplitude spectrum is defined as (Brune, 1970, 1971; Boore, 1983, 2003)

$$A(f) = \frac{R_{\theta\phi} F V M_0 (2\pi f)^2}{4\pi\rho\beta^3 \left[1 + \left(\frac{f}{f_0}\right)^2\right]}, \quad (11)$$

in which M_0 is the seismic moment; $R_{\theta\phi}$ is the radiation pattern average value of 0.55 for shear waves; F is the free-surface amplitude amplification equal to 2; V is the coefficient for partitioning into two horizontal components, $1/\sqrt{2}$; and ρ is the density, assumed to be 2800 kg/m^3 (Boore, 1983, 2003). The parameter f_0 is the source corner frequency given by

$$f_0 = 4.906 \times 10^3 \beta \left(\frac{\Delta\sigma}{M_0}\right)^{1/3}, \quad (12)$$

in which β is the shear-wave velocity at the source (taken as 3.51 km/s for this study) and $\Delta\sigma$ is the stress drop. The quality factor estimation is performed utilizing a wide range of stress drops (100–600 bars with 100 bars interval). It was observed that the assumed value of stress drop has negligible effect on the estimated quality factors at all frequencies; therefore, a typical stress drop of 100 bars is selected for all events.

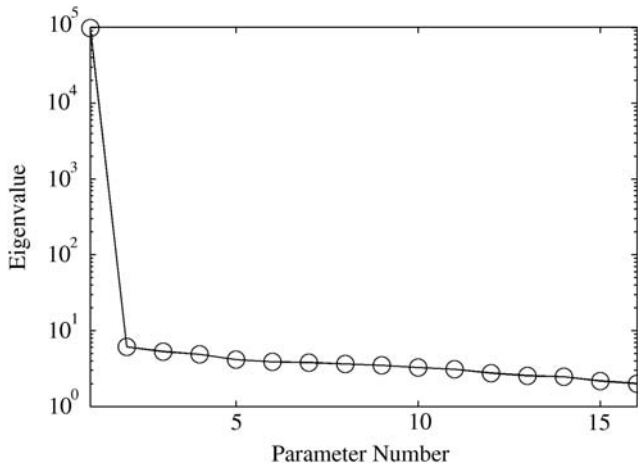


Figure 5. Eigenvectors for the forward operator \mathbf{G} , constructed from the horizontal components at 8.0 Hz.

Results and Discussion

Using equations (5)–(12), quality factors for vertical and horizontal components are estimated. Figure 7 illustrates the obtained frequency-dependent $Q(f)$; a straight line in logarithmic scale with equation $Q = Q_0 f^n$ is fitted to the quality factor estimates. The resulting equations are $Q^H = 310f^{0.54}$ for the horizontal component, and $Q^V = 235f^{0.65}$ for the vertical component.

To make a visual comparison of the observed data with the model obtained for the path effect, we reorder equation (5) to estimate the observed path effect. The observed path effect is derived by removing the source and site (receiver) terms from recorded amplitudes. The observed path effect is referred to as normalized amplitudes by Atkinson and Mereu (1992) and Zandieh and Pezeshk (2010), and is given by

$$\log[BC_OBS(f, R_{i,j})] = \log[A_i(f)] - \log[O_{i,j}(f)] + \log[S_j(f)], \quad (13)$$

in which $\log[BC_OBS(f, R_{i,j})]$ is the observed path effect. The predicted path effect is calculated by the following equation, assuming a geometrical spreading function and an estimated quality factor for different frequencies:

$$\log[BC_PRE(f, R_{i,j})] = B(R_{i,j}) \log(R_{i,j}) + \frac{\log(e)\pi f}{Q(f) \times \beta} R_{i,j}, \quad (14)$$

in which $\log[BC_PRE(f, R_{i,j})]$ is the predicted path effect and can be plotted along with the observed path effect given in equation (13). Furthermore, residuals are determined by

$$Res(f, R_{i,j}) = \log[BC_OBS(f, R_{i,j})] - \log[BC_PRE(f, R_{i,j})]. \quad (15)$$

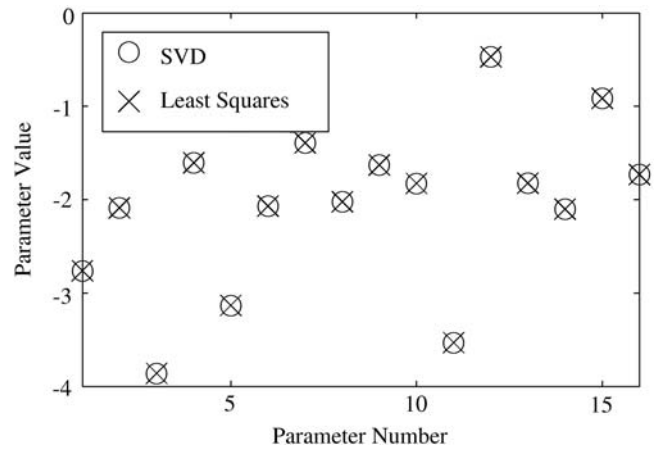


Figure 6. Solution of the singular value decomposition technique compared with the results of the conventional least squares. Parameters are the natural logarithm of the site (receiver) terms obtained from horizontal components at 8.0 Hz.

Figures 8 and 9 show observed and predicted path effects and residuals for frequencies of 1.0 and 4.0 Hz, associated with horizontal and vertical components. Other frequencies show the same trend and no irregular behavior is observed. There is no apparent trend in residuals versus distance; a straight line is fitted to the residuals, and the equation of the line, as presented in the residual plots, shows a minimum intercept and slope.

Summary and Conclusions

Only data with epicentral distances greater than 100 km were used. We assumed a geometrical spreading of $R^{-1.0}$ ($b_1 = 1.0$) for distances less than 75 km; for distances from 75 to 100 km, no decay is presumed ($b_2 = 0.$); and $R^{-0.5}$ ($b_3 = 0.5$) is assumed beyond 100 km. The following quality factor function and geometric pairs are obtained: $Q^H = 310f^{0.54}$ for the horizontal component, and $Q^V = 235f^{0.65}$ for the vertical component.

Figure 10 shows the attenuation models in the Caribbean region and the surrounding region, ranging from Jamaica and Cuba in the west to Puerto Rico and the Lesser Antilles in the east, compared to those in the WUS and CEUS regions. Both WUS and the Caribbean region have higher attenuation (lower Q factor) than the CEUS. Table 2 presents parameters used by various studies plotted in Figure 10. According to the observations, Q_0 in this study is close to those from the Hispaniola Island region (McNamara *et al.*, 2012) and Basin and Range Province (Benz *et al.*, 1997).

Hough and Anderson (1988) and McNamara *et al.* (2012) pointed out the attenuation properties of the Lg phase differ from those of the direct S wave because the Lg phase samples the entire crust, including the deeper crust, which is likely to be characterized by lower attenuation (higher Q factor), whereas the direct S waves are more controlled

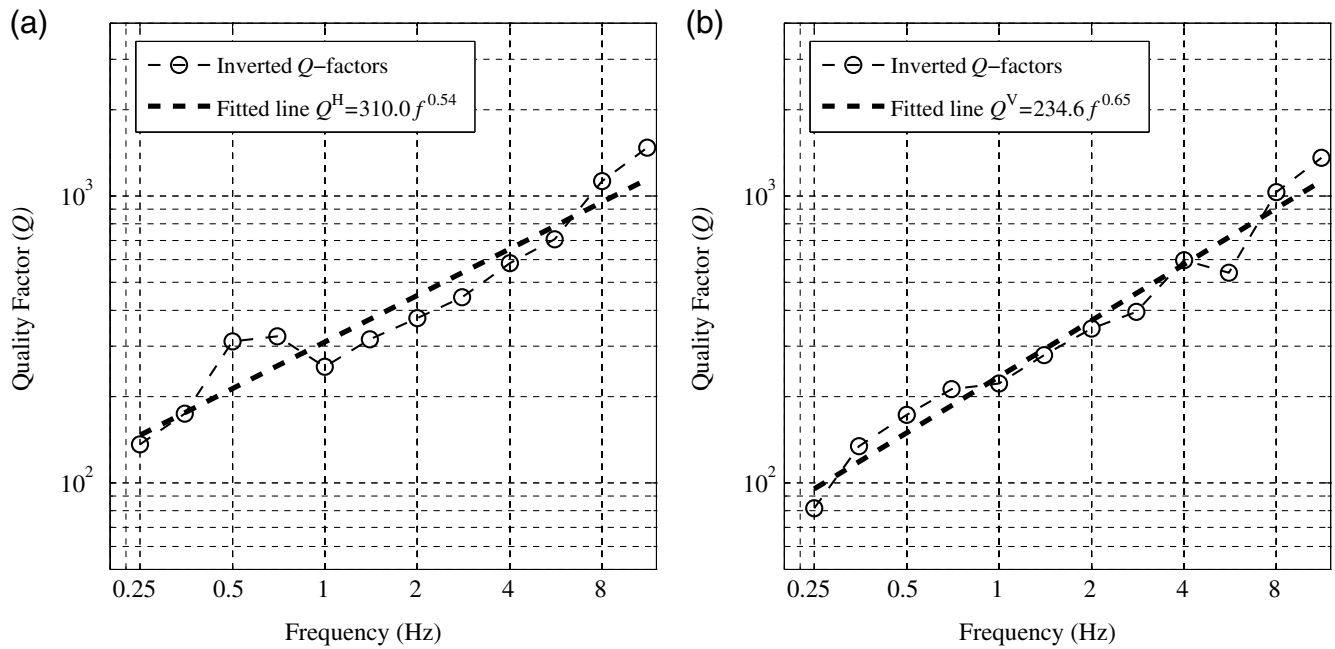


Figure 7. The quality factor versus frequency for (a) horizontal and (b) vertical components.

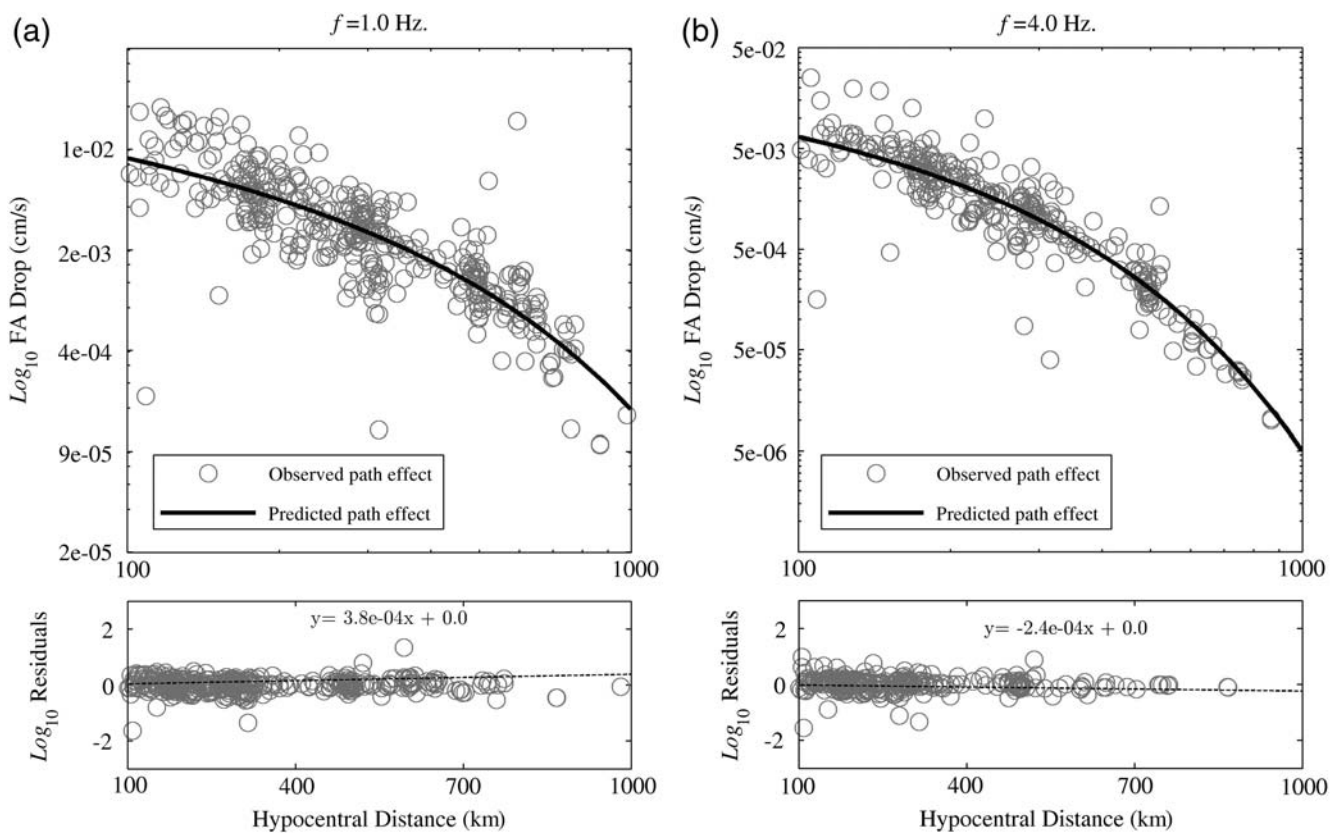


Figure 8. Fit quality between the predicted and observed path effects (top) and trend of the residuals (bottom) for frequencies (a) 1.0 Hz and (b) 4.0 Hz for horizontal amplitudes. A line is fitted to the residuals, and its equation is provided to quantitatively investigate the trend of the residuals.

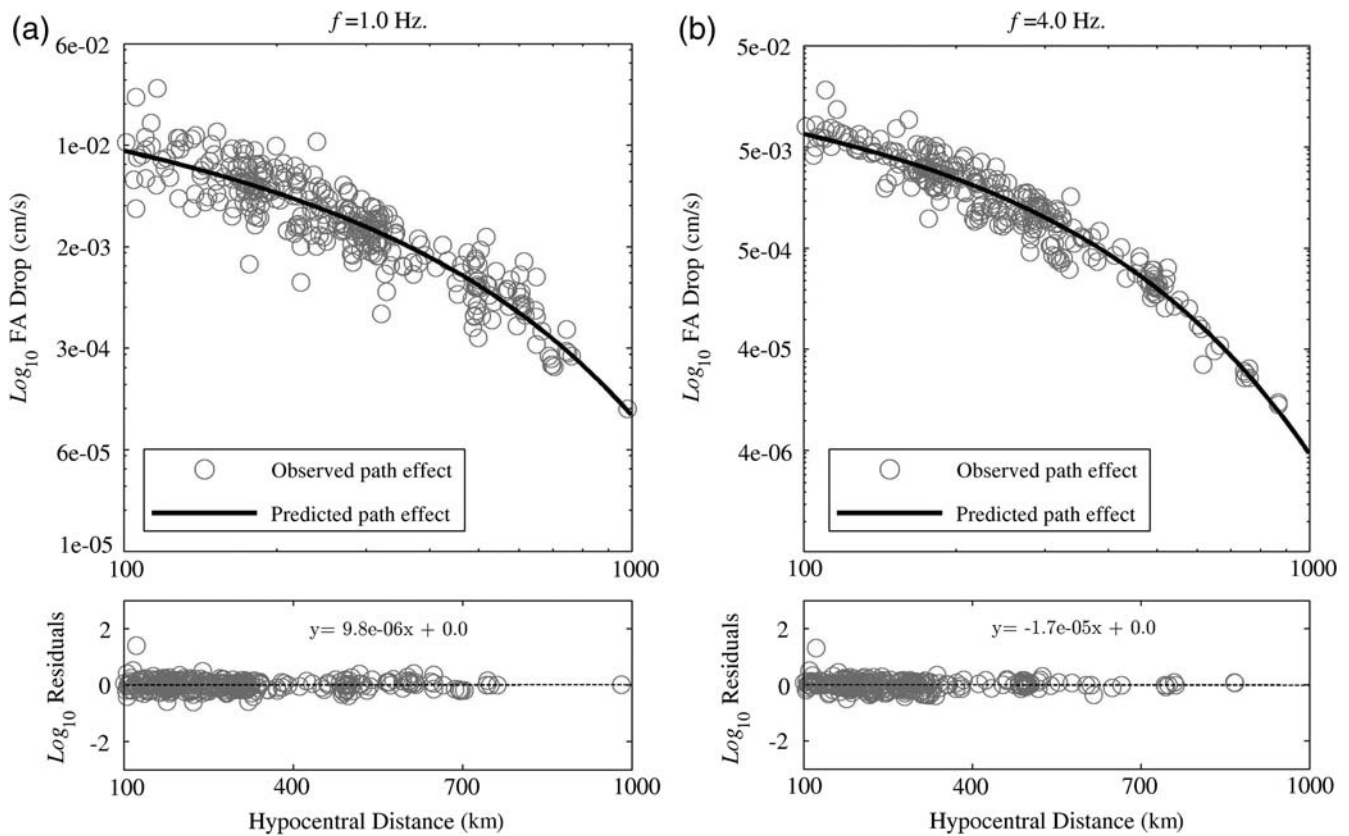


Figure 9. Similar to Figure 8 but for vertical components.

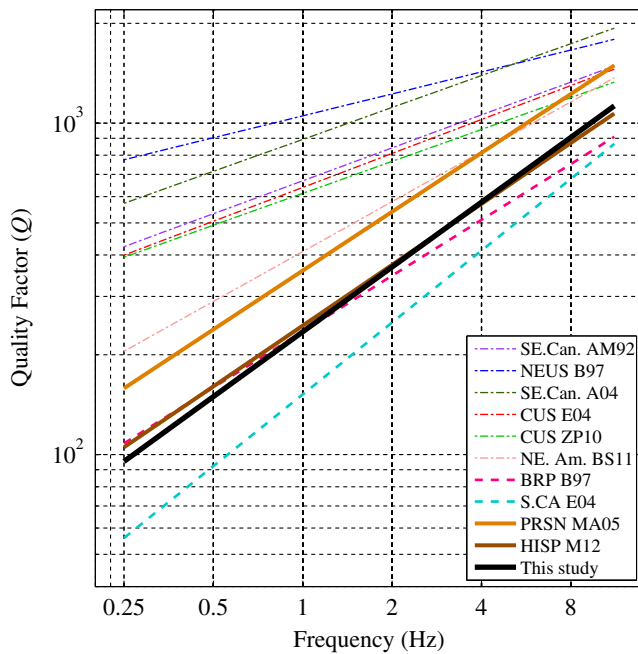


Figure 10. Comparison of quality factor from vertical components acquired in this study (solid thick line) with those reported by others. Abbreviations are used for the names of investigators and the region, as provided in Table 2. The color version of this figure is available only in the electronic edition.

by the upper crust (lower Q factor). Therefore, the Q -factor model developed by Motazedian and Atkinson (2005) for the Puerto Rico region using local earthquakes as deep as 200 km might give a higher Q factor (lower attenuation) than the shallow crustal attenuation models in the Caribbean region.

Data and Resources

All waveforms used in this study are archived and available for download from the Incorporated Research Institutions for Seismology Data Management Center. The data are all from broadband seismometers. Seismograms and all station instrument responses were received automatically using Standing Order of Data software. All three components of the waveforms are utilized in the analysis and only those stations were selected that simultaneously possessed components in three directions. Correction for the instrument response was performed using a modified version of the Engineering Seismology Toolbox developed by Assatourians and Atkinson (2008). Processing and inversion was performed using an automated package developed at the University of Memphis, Department of Civil Engineering, as a part of the Next Generation Attenuation-East project.

Table 2
Reported Parameters of Quality Factor $Q(f)$

| Number | Region | Q_0 | η | Source | Abbreviation |
|--------|----------------------------|-------|--------|--------------------------------|--------------|
| 1 | Southeastern Canada | 670 | 0.33 | Atkinson and Mereu (1992) | SE.Can. AM92 |
| 2 | Northeastern United States | 1052 | 0.22 | Benz <i>et al.</i> (1997) | NEUS B97 |
| 3 | Southeastern Canada | 893 | 0.32 | Atkinson (2004) | SE.Can. A04 |
| 4 | Central United States | 640 | 0.34 | Erickson <i>et al.</i> (2004) | CUS E04 |
| 5 | Central United States | 614 | 0.32 | Zandieh and Pezeshk (2010) | CUS ZP10 |
| 6 | Northeastern America | 410 | 0.50 | Boatwright and Seekins (2011) | NE.Am. BS11 |
| 7 | Basin and Range Province | 235 | 0.56 | Benz <i>et al.</i> (1997) | BRP B97 |
| 8 | Southern California | 152 | 0.72 | Erickson <i>et al.</i> (2004) | S.CA E04 |
| 9 | Puerto Rico | 359 | 0.59 | Motazedian and Atkinson (2005) | PRSN MA05 |
| 10 | Hispaniola | 245 | 0.61 | McNamara <i>et al.</i> (2012) | HISP M12 |
| 11 | Caribbean | 235 | 0.65 | This study | — |

Acknowledgments

We wish to thank Dariush Motazedian and an anonymous reviewer for their comments, suggestions, and helpful criticisms that greatly improved the manuscript.

References

- Aki, K. T. (1980a). Attenuation of shear-waves in the lithosphere from frequencies from 0.05 to 25 Hz, *Phys. Earth Planet. In.* **21**, 50–60.
- Aki, K. T. (1980b). Scattering and attenuation of shear-waves in the lithosphere, *J. Geophys. Res.* **85**, 6496–6504, doi: [10.1029/JB085iB11p06496](https://doi.org/10.1029/JB085iB11p06496).
- Aki, K. T., and P. G. Richards (1980). *Quantitative Seismology*, Freeman and Co., New York, New York.
- Allen, T. I., P. R. Cummins, T. Dhu, and J. F. Schneider (2007). Attenuation of ground-motion spectral amplitudes in southeastern Australia, *Bull. Seismol. Soc. Am.* **97**, 1279–1292.
- Ambe, W. B., and L. L. Lynch (1993). Coda Q in the eastern Caribbean, West Indies, *J. Geophys. Res.* **112**, 507–516.
- Assatourians, K., and G. M. Atkinson (2008). *Program: ICORRECT*, Report, University of Western Ontario, London, Ontario, Canada (CAN), <http://www.seismotoolbox.ca/ICORRECT/ICORRECT.pdf> (last accessed January 2012).
- Aster, R. C., B. Borchers, and C. H. Thurber (2013). *Parameter Estimation and Inverse Problems*, Second Ed., Elsevier Academic Press, Amsterdam, The Netherlands.
- Atkinson, G. M. (2004). Empirical attenuation of ground motion spectral amplitudes in southeastern Canada and the northeastern United States, *Bull. Seismol. Soc. Am.* **94**, 1079–1095.
- Atkinson, G. M. (2012). Evaluation of attenuation models for the northeastern United States/southeastern Canada, *Seismol. Res. Lett.* **83**, 166–178.
- Atkinson, G. M., and D. M. Boore (1995). Ground-motion relations for eastern North America, *Bull. Seismol. Soc. Am.* **85**, 17–30.
- Atkinson, G. M., and D. M. Boore (1998). Evaluation of models for earthquake source spectra in eastern North America, *Bull. Seismol. Soc. Am.* **88**, 917–934.
- Atkinson, G. M., and D. Boore (2006). Ground motion prediction equations for earthquakes in eastern North America, *Bull. Seismol. Soc. Am.* **96**, 2181–2205.
- Atkinson, G., and R. Mereu (1992). The shape of ground motion attenuation curves in southeastern Canada, *Bull. Seismol. Soc. Am.* **82**, 2014–2031.
- Båth, M. (1954). The elastic waves Lg and Rg along Euroasiatic paths, *Arkiv Geofysik (Stockholm)* **2**, 295–324.
- Benz, H., A. Frankel, and D. Boore (1997). Regional Lg attenuation for the continental United States, *Bull. Seismol. Soc. Am.* **87**, 606–619.
- Boatwright, J., and L. C. Seekins (2011). Regional spectral analysis of three moderate earthquakes in northeastern North America, *Bull. Seismol. Soc. Am.* **101**, 1769–1782.
- Bollinger, G. A. (1979). Attenuation of Lg phase and the determination of m_b in the southeastern United States, *Bull. Seismol. Soc. Am.* **69**, 45–63.
- Boore, D. M. (1983). Stochastic simulation of high-frequency ground motions based on seismological models of the radiated spectra, *Bull. Seismol. Soc. Am.* **73**, 1865–1894.
- Boore, D. M. (2003). Simulation of ground motion using the stochastic method, *Pure Appl. Geophys.* **160**, 635–676.
- Brune, J. (1970). Tectonic stress and the spectra of seismic shear-waves from earthquakes, *J. Geophys. Res.* **75**, 4997–5009.
- Brune, J. (1971). Correction, *J. Geophys. Res.* **76**, 5002.
- Calais, E., A. Freed, G. Mattioli, F. Amelung, S. Jónsson, P. Jansma, T. Dixon Sang-Hoon Hong, C. Pfeppit, and R. Momplaisir (2010). Transpressional rupture of an unmapped fault during the 2010 Haiti earthquake, *Nature Geosci.* **3**, 794–799.
- Chapman, M. C., and R. W. Godbee (2012). Modeling geometrical spreading and the relative amplitudes of vertical and horizontal high-frequency ground motions in eastern North America, *Bull. Seismol. Soc. Am.* **102**, 1957–1975.
- Chen, T. C., and P. W. Pomeroy (1980). Regional seismic wave propagation, *Semi-Annual Technical Report No. 5*, Rondout Associates, Inc., Stone Ridge, New York.
- Clinton, J. F., G. Cua, V. Huérano, C. von Hillebrandt-Andrade, and J. Martínez-Cruzado (2006). The current state of seismic monitoring in Puerto Rico, *Seismol. Res. Lett.* **77**, no. 5, 532–543.
- Erickson, D., D. E. McNamara, and H. M. Benz (2004). Frequency dependent Lg Q within the continental United States, *Bull. Seismol. Soc. Am.* **94**, 1630–1643.
- Frankel, A. (1982). The effects of attenuation and site response on the spectra of microearthquakes in the northeastern Caribbean, *Bull. Seismol. Soc. Am.* **72**, 1379–1402.
- Frankel, A. (1991). Mechanisms of seismic attenuation in the crust: Scattering and anelasticity in New York state, South Africa, and southern California, *J. Geophys. Res.* **96**, 6269–6289.
- Frankel, A., A. McGarr, J. Bicknell, J. Mori, L. Seeber, and E. Cranswick (1990). Attenuation of high-frequency shear waves in the crust: Measurements from New York state, South Africa, and southern California, *J. Geophys. Res.* **95**, doi: [10.1029/JB095iB11p17441](https://doi.org/10.1029/JB095iB11p17441).
- Frankel, A., C. Mueller, T. Barnhard, D. Perkins, E. Leyendecker, N. Dickman, S. Hanson, and M. Hopper (1996). Documentation for the 1996 update of the United States national seismic hazard maps, *U.S. Geol. Surv. Open-File Rept.* 1996-532.
- Gregersen, S. (1984). Lg wave propagation and crustal structure differences near Denmark and the North Sea, *Geophys. J. Int.* **79**, 217–234.
- Hough, S. E., and J. G. Anderson (1988). High-frequency spectra observed at Anza, California: Implications for Q structure, *Bull. Seismol. Soc. Am.* **78**, 692–707.
- Jackson, T. A. (Editor) (2002). *Caribbean Geology: Into the Third Millennium*, Transactions of the 15th Caribbean Geological Conference, The

- University of the West Indies Press, Kingston, Jamaica, 29 June–2 July 1998, 287 pp.
- Kennett, B. (1986). *Lg* waves and structural boundaries, *Bull. Seismol. Soc. Am.* **76**, 1138–1141.
- Lay, T., and T. C. Wallace (1995). *Modern Global Seismology*, Academic Press, New York, New York, 243–249.
- Mattson, P. H. (Editor) (1977). *West Indies Island Arcs*, Benchmark Papers in Geology 33, Dowden, Hutchinson and Ross, Inc., London, United Kingdom, 361 pp.
- McNamara, D., M. Meremonte, J. Z. Maharrey, S.-L. Mildore, J. R. Altdore, D. Anglade, S. E. Hough, D. Given, H. Benz, L. Gee, and A. Frankel (2012). Frequency-dependent seismic attenuation within the Hispaniola Island region of the Caribbean Sea, *Bull. Seismol. Soc. Am.* **102**, 773–782.
- Menke, W. (1984). Asymptotic formulas for the apparent *Q* of weakly scattering three dimensional media, *Bull. Seismol. Soc. Am.* **74**, 1079–1081.
- Mitchell, B. J. (1975). Regional Rayleigh wave attenuation in North America, *J. Geophys. Res.* **80**, 4904–4976.
- Mitchell, B. J. (1995). Anelastic structure and evolution of the continental crust and upper mantle from seismic surface wave attenuation, *Rev. Geophys.* **33**, 441–462.
- Molnar, P., and J. Oliver (1969). Lateral variations of attenuation in the upper mantle and discontinuities in the lithosphere, *J. Geophys. Res.* **74**, 2648–2682.
- Motazedian, D., and G. M. Atkinson (2005). Ground-motion relations for Puerto Rico, in *Active Tectonics and Seismic Hazards of Puerto Rico, the Virgin Islands, and Offshore Areas*, P. Mann (Editor), *Geol. Soc. Am. Spec. Pap.* **385**, 61–80.
- Nicolas, M., B. Massinon, P. Mechler, and M. Bouchon (1982). Attenuation of regional phases in western Europe, *Bull. Seismol. Soc. Am.* **72**, 2089–2106.
- Nuttli, O. W. (1973). Seismic wave attenuation and magnitude relations for eastern North America, *J. Geophys. Res.* **78**, 876–885.
- Odum, J. K., W. J. Stephenson, R. A. Williams, and C. V. Hillebrandt-Andrade (2013). V_{530} and spectral response from collocated shallow, active- and passive-source V_S data at 27 sites in Puerto Rico, *Bull. Seismol. Soc. Am.* **103**, 2709–2728.
- Pezeshk, S., A. Zandieh, and B. Tavakoli (2011). Hybrid empirical ground-motion prediction equations for eastern North America using NGA models and updated seismological parameters, *Bull. Seismol. Soc. Am.* **101**, no. 4, 2709–2728.
- Press, F., and M. Ewing (1952). Two slow surface waves across North America, *Bull. Seismol. Soc. Am.* **42**, 219–228.
- Rial, J. A. (1976). Seismic-wave transmission across the Caribbean plate: High attenuation on concave side of Lesser Antilles island arc, *Bull. Seismol. Soc. Am.* **66**, 1905–1920.
- Singh, S., and R. B. Herrmann (1983). Regionalization of crustal code *Q* in the continental United States, *J. Geophys. Res.* **88**, 527–538.
- Toro, G. R., N. A. Abrahamson, and J. F. Schneider (1997). A model of strong ground motions from earthquakes in central and eastern North America: Best estimates and uncertainties, *Seismol. Res. Lett.* **68**, 41–57.
- Zandieh, A., and S. Pezeshk (2010). Investigation of geometrical spreading and quality factor functions in the New Madrid seismic zone, *Bull. Seismol. Soc. Am.* **100**, no. 5, 2185–2195.
- Zhou, L., C. Zhao, Z. Chen, and S. Zheng (2011). Amplitude tomography of *Lg* waves in Xinjiang and its adjacent regions, *Bull. Seismol. Soc. Am.* **101**, no. 3, 1302–1314.

Department of Civil Engineering
The University of Memphis
Memphis, Tennessee 38152
(M.H., S.P., A.H.-S.)

Department of Geosciences
Virginia Polytechnic Institute and State University
Blacksburg, Virginia 24061
(M.C.)

Manuscript received 7 January 2014;
Published Online 27 January 2015